ELECTRICAL DECAY ESTIMATES IN ANVIL CLOUDS

Report No. 1 of 2 under Contract No. CC-90233B

John C. Willett, 12/28/01

Introduction

The purpose of this investigation is to aid NASA and the USAF in determining when cirrus anvils do not constitute a triggered-lightning hazard for either an outgoing launch vehicle or a landing Space Shuttle. The "Anvil Clouds" Rule in the current Launch-Commit Criteria (LCC) prohibits penetration of non-transparent parts of an anvil cloud while it remains attached to its parent cloud and for the first 3 hours after detachment is observed (or for the first 4 hours after the last lightning discharge occurs in the detached anvil cloud) [*Krider et al.*, 1999]. This rule causes significant launch delays and scrubs in conditions that are probably (but are not *known* to be) safe. One such condition that occurs at the Kennedy Space Center (KSC) during the early spring is a translucent cirrus shield formed by blow-off from a distant mesoscale convective complex over the eastern Gulf of Mexico.

Beginning in the summer of 2000 and extending into the summer of 2001, an Airborne Field Mill (ABFM) experiment has been conducted in the vicinity of KSC to measure both the ambient electrostatic fields and the size/shape distributions of the cloud and precipitation particles in cirrus anvils (as well as in and near other cloud types). One important goal of this field experiment was to obtain data on the decay of electric fields within anvil clouds as they age after detachment or are advected downstream from their parent cumulonimbus clouds. It was hoped that these observations, coupled with a means of remotely assessing the microphysics of these clouds from the ground, would allow a description of hazardous anvils that was much more restricted than the one in the existing "Anvil Clouds" rule. If the observations could also be used to validate a simple theory of how electric fields *should* decay in anvil cirrus, then a relatively small number of observations could yield sufficient confidence to permit the safe relaxation of this launch constraint.

The work described herein is intended to articulate the simple theoretical model mentioned above and to insert preliminary ABFM microphysical measurements into this model in order to predict the decay times of electric fields within an actual anvil cloud. These decay times could then be compared with ABFM ambient-field observations in the same clouds in an effort to validate the theory.

Theoretical Model

The simplest possible model of a charged cirrus anvil is a one-dimensional structure with constant microphysics but time-dependent electrification. Imagine a horizontally homogeneous cloud of constant thickness, H (m), and of uniform cloud-particle size and shape distributions that initially contains a layer of positive electric charge residing on particles at its center and having area density, σ_0 (C m^{-2}). (All units in this report are rationalized MKS. All references to cloud particles should be taken to connote the whole range of hydrometeors, from the smallest frozen cloud droplets to the largest aggregates.) We assume an all-ice cloud with no sedimentation, aggregation, convection, nor any other active processes that might generate further electrification.

If H is large enough, and if there is no turbulent mixing, screening layers of negative charge will form rapidly on the upper and lower surfaces of this cloud, confining the elevated electric fields between the cloud boundaries [*Brown et al.*, 1971; *Hoppel and Phillips*, 1971; *Klett*, 1972]. For simplicity we imagine the internal charge layer and the two screening layers (each of area density, $-\sigma_0/2$) to be infinitely thin; so that the entire cloud volume is filled with a uniform electric field intensity, $E_0 = \sigma_0/(2\varepsilon_0)$ (V m^{-1}), of positive polarity (upward-directed) above the cloud center and negative (downward) below, where ε_0 (F m^{-1}) is the dielectric permittivity of free space. These are the initial conditions for our simple model of the time evolution of $E(t)$. This evolution could apply equally to the temporal decay of field within a stationary detached anvil or (with substitution, $t = x/v$, where x is distance in the down-stream direction and v is horizontal advection speed) to the spatial decay of field in an attached anvil down wind from the parent cloud.

Small ions are constantly created in pairs within the cloud, primarily by cosmic radiation at the altitudes of typical cirrus anvils, at the volume production rate, q (m^{-3} s^{-1}). These ions drift parallel to the ambient field with electrical mobility, k (m^2 V^{-1} s^{-1}), resulting in a current density, $J(t) = 2ekn(t)E(t)$ (A m^{-2}), that tends to neutralize simultaneously all three charge layers in the cloud. Here, e (C) is the electronic charge and $n(t)$ (m^{-3}) is the volume density of both positive and negative small ions (assumed equal). By charge continuity and the above relationships, $J(t)$ leads to a decay of the field intensity within the cloud, as follows:

$$dE/dt = -2ekn(t)E(t)/\varepsilon_0 \qquad (1)$$

Note that a macroscopic, continuum approach has been used to compute electrical conduction and electric-field decay inside the cloud, in spite of the fact that nearly all charge actually resides on cloud particles. The main justification for this approach is that, in order to eliminate the macroscopic electric fields of concern for launch safety, we do not care whether or not the charge on individual particles is neutralized. It is sufficient that the large-scale, net-charge density be neutralized, and this may be accomplished by macroscopic conduction currents mediated by a bulk "conductivity." For these purposes the deposition of opposite charge on other particles within the same macroscopic cloud volume is equivalent to neutralization of the initially charged particles.

We implicitly allow the positive and negative small-ion densities to diverge and to have strong gradients near the surfaces of individual cloud particles when computing the attachment rates of ions to particles, below. This does not invalidate the macroscopic calculation in Equation 1, however, as long as the fraction of cloud volume occupied by particles is negligibly small. We will, in fact, assume that the particles are far enough apart that the ion-density gradients produced by one particle do not affect the attachment rates at another.

Were $n(t)$ constant, as it normally is in the free atmosphere, the solution of (1) would yield the familiar exponential decay of $E(t)$ according to the "electrical relaxation time," $\tau_e = \varepsilon_0/(2ekn)$ (s), for the relevant altitude. ($\tau_e \approx 19$ s at an altitude of 10 km in the free atmosphere, which is utterly negligible from the perspective of launch safety.) In addition to the usual ion-loss processes of recombination and aerosol attachment (neither of which depends significantly on E, and both of which will be neglected here), however, small ions may both diffuse to and be electrically driven to the cloud particles, where they are annihilated. The latter process is field dependent and is always the dominant loss mechanism at sufficiently high field intensities. Thus, in order to solve (1), we must first compute $n(t)$ in the cloud as a function of both the microphysics and the time-dependent field.

The motivation for this analysis was a suggestion by *Krehbiel* [1998]. Related to earlier work by *Gunn* [1954, 1956], *Krehbiel* [1967] had shown that cloud "conductivity" (non-Ohmic in this case) should become independent of k, and that $J(t)$ should become constant -- independent of both k and $E(t)$ -- when the ambient field is strong enough. The basic reason for this simplification is that small ions, drifting through the cloud in response to the ambient field, are "swept out" by the effective cross-section area of the particles at a rate proportional to field intensity and ion mobility. Since the conduction-current

density is also proportional to these two parameters, their effects cancel out in strong electric fields.

The present starting point is the steady-state small-ion-budget equation in a population of stationary, non-interacting, mono-disperse, spherical, electrically-conducting cloud particles [*Pruppacher and Klett*, 1978, Eq. 17-40]. After neglecting small-ion recombination, this equation has been simplified to consider only uncharged cloud particles and has been generalized to account for non-spherical (ice) particles. The simplification is justified for an ensemble of initially uncharged particles in air of approximately equal, polar, small-ion densities by the modeling results of *Griffiths et al.* [1974]. The generalization is based on the well-known analogy between the diffusive flux to an isolated object and its electrical capacitance, C (F) [*e.g.*, *Pruppacher and Klett*, 1978, Section 13.3.1] -- $C = 2\pi\varepsilon_0 y$ for a sphere of diameter, y (m). The "Einstein relation" [*e.g.*, *Pruppacher and Klett*, 1978, Eq. 12-21] has also been used to replace the ionic diffusivity with k in the second term on the right-hand side:

$$q \approx A_e k N n(t) E(t) + (C/\varepsilon_0)(kKT/e) N n(t), \qquad (2)$$

The steady-state assumption (that $dn/dt \approx 0$ in the small-ion budget equation) is valid to the extent that the time scales of interest are long compared to the small-ion lifetime, $\tau_i = n/q$ (s). An upper bound can be placed on τ_i by setting the (neglected) ion-ion recombination-loss rate equal to q. At an assumed altitude of 10 km, this results in $\tau_i \approx 140$ s, which is certainly negligible from the point of view of launch safety.

The first term on the right of (2) is the small-ion loss rate due to field-driven attachment of ions to cloud particles, where A_e (m^2) is the effective electrical cross section of a particle -- $A_e = 3\pi y^2/4$ for a sphere -- and N (m^{-3}) is their volume concentration. The second term is the diffusive loss rate, where K (J $Kelvin^{-1}$) is the Boltzmann constant and T (Kelvin) is the absolute temperature. Since each of these terms is linear in N, the particle concentration can be replaced with a size distribution, $N(y)$ (m^{-3} m^{-1}) (taken to extend from the smallest ice crystals to the largest aggregates present in the cloud), both A_e and C can be made functions of y, and the right-hand side of (2) can then be integrated over y to obtain the total ion-loss rate. For non-spherical particles, A_e and C also become functions of particle shape. If the particles can be represented by prolate spheroids, then

$$A_e\,(y,\ r)\ =\ \frac{\pi\,[1\ -\ \frac{1}{r^2}\,]\,y^2}{2\,\left[-2\ +\ \frac{2\ r\,\mathrm{Ln}\,\left(r+\sqrt{-1+r^2}\right)}{\sqrt{-1+r^2}}\right]} \qquad (3)$$

$$C\,(y,\ r)\ =\ \frac{2\,\pi\,\sqrt{-1\ +\ r^2}\ y\ \varepsilon_0}{r\,\mathrm{Ln}\,\left(r\ +\ \sqrt{-1\ +\ r^2}\right)} \qquad (4)$$

where y is now the length of the major axis (assumed to be oriented by electrical forces to lie parallel to the electric-field direction) and r is the ratio of major- to minor-axis lengths. Further choices for particle shape can be found in *Richards et al.* [1981]. For example, if the particles are hexagonal plates (r = 21.9 is now the ratio of width to thickness) oriented edge-on to the field direction, then in the present notation, $A_e(y) = 1.35y^2$ and $C(y) = 4.52\varepsilon_0 y$.

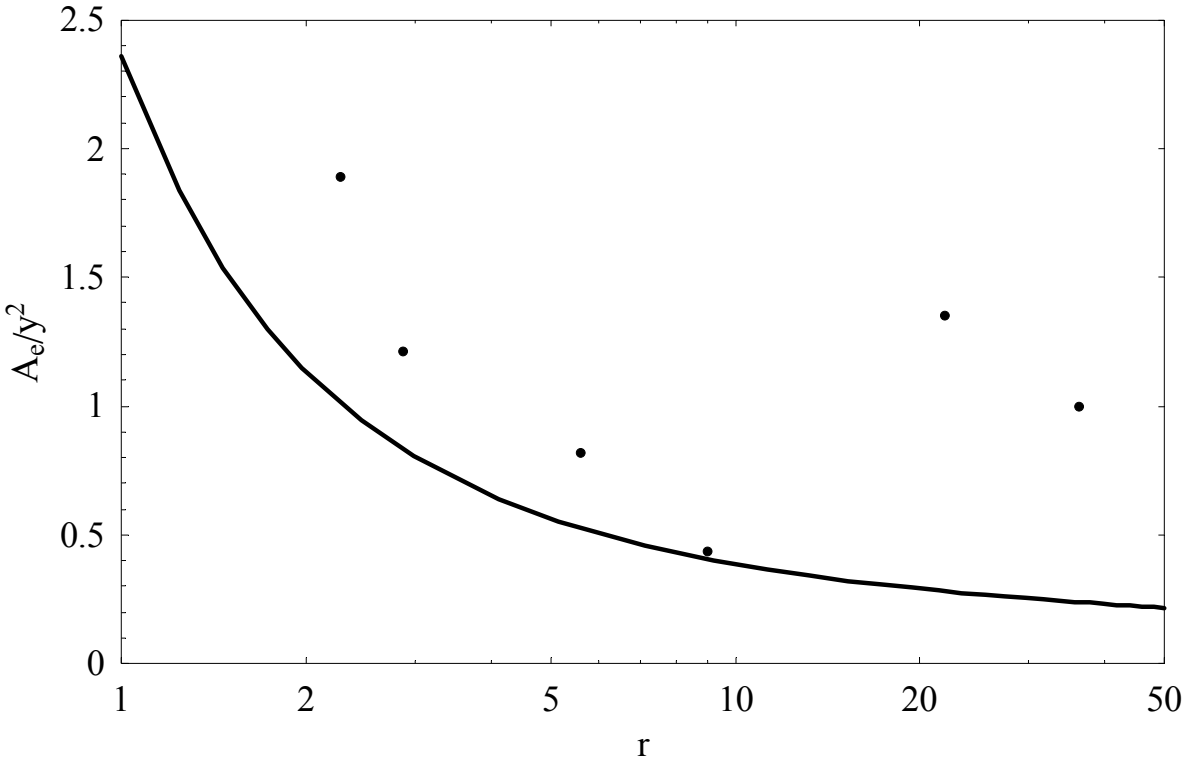

Figure 1 -- Dependence of dimensionless electrical effective area on particle shape for prolate spheroids and for selected shapes from *Richards et al.* [1981]

Notice that A_e varies approximately quadraticly with the particle's long dimension, y, whereas C is approximately linear in y, these proportionalities being exact for constant r. Thus,

field-driven attachment of ions to particles will dominate diffusive attachment at the larger sizes. Figure 1 shows the dependence of dimensionless A_e/y^2 on particle shape (expressed by the ratio of long to short dimension, r). Here the curve applies to prolate spheroids (3), while the points apply, in order of increasing r, to the particle shapes that have been called column1, bullet, column2, needle, plate (see text above), and dendrite by *Richards et al*. [1981]. The value, $A_e/y^2 = 3\pi/4$, for $r = 1$ applies to the sphere. Although A_e decreases rapidly as r increases from 1 to 2, the dependence on shape (or short dimension, for constant y) becomes weak for the highly elongated particles. The prolate shapes of *Richards et al*. [1981] (column1, bullet, column2, and needle), fit the spheroid formula fairly well; not surprisingly, the oblate (but edge-on to the field) shapes (plate and dendrite) do not.

Figure 2 shows the dependence of dimensionless $C/(\varepsilon_0 y)$ on r, with the curve from Equation 4. The value, $C/(\varepsilon_0 y) = 2\pi$, for $r = 1$ applies to the sphere. Most of the comments regarding Figure 1 apply here as well, except that the dependence of C on r is never very strong.

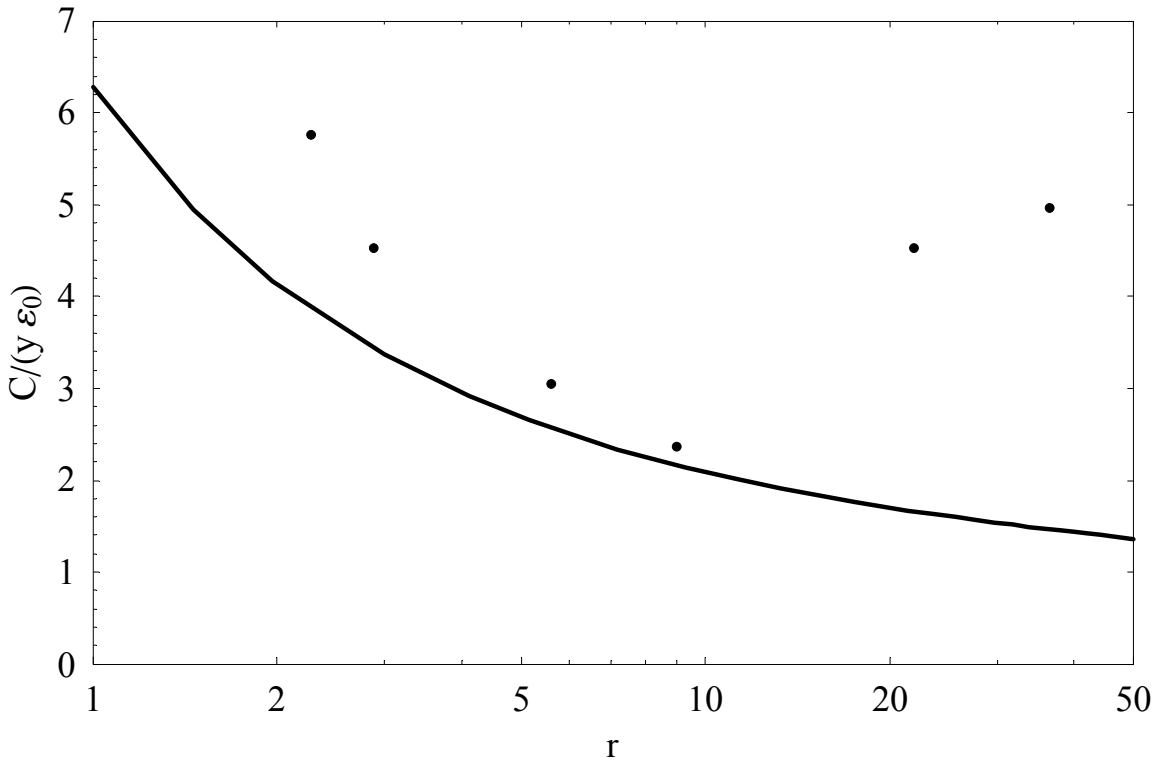

Figure 2 -- Dependence of dimensionless capacitance on particle shape for prolate spheroids and for selected shapes from *Richards et al*. [1981]

Given the relatively poor electrical conductivity of ice (a well-known issue for the ice-ice inductive-electrification mechanism [*e.g.*, *Latham and Mason*, 1962]), it is worth pointing out that cloud particles can still be considered excellent conductors in the present context. The steady-state surface-charge density on an isolated body exposed to an ambient field in air will deviate from that on a perfect conductor of the same shape in proportion to the ratio of the air's conductivity to that of the body. The bulk conductivity of pure ice at the low temperatures of cirrus anvils (a worst case, since surface conductivity, enhanced by impurities, is the dominant mechanism on real cloud particles [*Gaskell*, 1981; *Caranti and Illingworth*, 1983]) can be estimated from the data of *Gross* [1982], who measured relaxation times on the order of 5 ms. If we assume a dielectric constant for ice of order 100, this bulk conductivity is of order 2×10^{-7} S/m. In contrast, the conductivity of the free atmosphere at 10 km altitude (again a worst case, since the cloud conductivity will be less) is of order 5×10^{-13} S/m. Thus, the ratio in question must be infinitesimal.

The condition of approximately equal diffusive and field-driven ion-loss rates in (2) can be identified by a value of unity for the dimensionless parameter, $\gamma = A_e e \varepsilon_0 E/(CKT)$, which is essentially the same as Equation 5 of *Klett* [1971]. When $\gamma \gg 1$, we are in the "high-field limit," which will be of most concern here because the decay of electrification can become quite slow. It is easy to see from (1) and (2) that $dE/dt \approx -2eq/(A_e \varepsilon_0 N)$ in this limit, as pointed out by *Krehbiel* [LAP meeting, Tucson, AZ, January, 1998]. When $\gamma \ll 1$, on the other hand, the "low-field limit" obtains, and molecular diffusion is the dominant loss mechanism (unless the cloud is fairly sparse, in which case the neglected ion-ion recombination process becomes significant). This limit yields exponential decay of $E(t)$ with a "diffusive relaxation time," $\tau_D = CKTN/(2e^2 q)$ (s), which is valid only if it is much longer than τ_e.

Equation 2 is not quite correct when $\gamma \approx 1$ because diffusion of small ions to a particle tends to diminish the field-driven loss rate to that particle. *Klett* [1971] analyzed this situation theoretically, however, and concluded that (2) provides a good approximation for practical purposes.

Here we work directly with (2), instead of focusing on the limiting cases mentioned above. Since both of the loss terms on the right-hand side are linear in ion density, it is trivial to solve this equation for $n(t)$ and substitute the result into (1) to obtain

$$dE/dt = -2eq\{\varepsilon_0 N[A_e + CKT/(\varepsilon_0 eE(t))]\}^{-1} \qquad (5)$$

where the denominator on the right-hand side is to be regarded as an integral over the particle size and shape distribution, as discussed above. (If ion-ion recombination had been retained as a third loss term in (2), we still could have solved the resulting quadratic equation for $n(t)$ and inserted it into (1). This additional complexity is not justified, however, since recombination is only important when the electric-field decay time approaches τ_e -- much shorter than anything relevant to launch safety.)

Screening Layers and Other Complications

Klett [1972] has shown that the thickness of the screening layer that builds up just inside a stationary cloud boundary perpendicular to the ambient electric field (in the absence of convection, turbulent mixing, evaporation, etc.) is $h \approx 1.85/(A_e N)$ (m), and that the time scale for development of this layer is $\tau_s \approx 4\tau_e$. In order for the present analysis to be valid, we require $h \ll H$, and τ_s must be small compared to the time scales of interest. The former will generally be true in thick and/or dense clouds, and the latter will be true (in high clouds such as anvils) whenever the field-decay time is long enough to become a cause for concern. If the screening layer thickness becomes comparable to, or larger than, the cloud thickness, however, the field-decay time will be reduced. Thus, the neglect of this condition is conservative.

The effects of turbulent mixing within the cloud are more difficult to quantify, but this complication is expected always to accelerate the decay of electrification, so the estimates made herein may be considered conservative in this regard as well. Similarly, we expect evaporation, aggregation, and fall-out of the larger particles all to change the size distribution in the direction of reducing the electrical-decay time scale.

Gravitational sedimentation of the cloud particles, on the other hand, introduces a "ventilation" correction to the diffusive loss term in (2) that increases the loss rate, the more significantly the larger (hence, the more rapidly falling) the particles [*e.g., Gunn*, 1954]. This is because the air flow around a falling particle tends to concentrate the ion-density gradient, especially near its lower surface, thereby increasing the diffusive flux. Assessment of the effects of this ventilation correction, if any, will be deferred to the second and final report on this contract.

Particle ventilation also has an effect on the field-driven loss term, but in the direction of reducing the ion-loss rate. When the terminal velocity of an uncharged particle exceeds the

ion-drift velocity in a vertical ambient field, the particle collects ions of one polarity on its lower surface, while ions of the opposite polarity are convected away before they can be collected on its upper surface. This is the well-known *Wilson* [1929] selective-ion-capture process. The particle charges up to a steady-state level at which it is collecting ions of both polarities at an equal rate. *Whipple and Chalmers* [1944] showed that, for a rapidly falling spherical particle in Stokes flow, the ion loss rate at equilibrium is just 69% of that if the particle were motionless (as assumed in Equation 2). This complication will be ignored here both because the Wilson mechanism does not operate on very many particles at the high fields of interest to launch safety and because any resulting error will be on the conservative side.

The most serious complication to the present analysis is the possibility that an active electrification mechanism might be operating within the cloud. The treatment of electrification mechanisms is beyond the scope of this contract. Since this would be likely in a mixed-phase cloud, however, where riming, vapor deposition, and collisions between ice particles with different temperatures and/or growth histories can occur, any evidence of liquid water in an anvil cloud should be cause for alarm.

Results from the ABFM June, 2000, Deployment

Equation 5 has been solved numerically in *Mathematica* (TM), after numerical integration of the denominator over the observed particle-size distribution, for several passes from the 13 June 2000 flight of the ABFM. (The *Mathematica* [TM] code is available upon request.) The day to focus on, as well as many of the times chosen here for analysis, were recommended to the author by Jim Dye [personal communication, November, 2001], based on his extensive survey of the experimental program and his in-depth analysis of this particular storm. The size distributions used were kindly provided by Jim Dye and Bill Hall of NCAR [personal communication, November-December, 2001]. In the present analysis all particles are taken to be spherical -- the most conservative assumption since it exaggerates both diffusive and electrically driven small-ion losses, yielding the longest electrical decay time for a given size spectrum. (This is a reasonable assumption for particles smaller than about 100 μm, which appear to be mostly frozen cloud droplets [Jim Dye, personal communication, November, 2001], but it could easily be relaxed as better information on the shapes of the larger particles becomes available.) The only other required inputs

are the ionization rate, taken as a function of altitude from *Hake et al.* [1973, Figure 19], the absolute temperature from the U.S. Standard Atmosphere, and (for explicit loss-rate calculations only, *e.g.*, Figures 5 & 10) the small-ion mobility, scaled in inverse proportion to atmospheric density from the U.S. Standard Atmosphere. At an altitude of 10 km, for example, these parameters become q = 3.0 X 10^7 pairs/m^3/s, T = 223 K, and k = 3.3 X 10^{-4} m^2/V/s.

During June, 2000, the High Volume Particle Sampler (HVPS, which effectively counts particles larger than roughly 1 mm) was not working properly, and data from the Cloud Particle Imager (CPI) has yet to be fully analyzed [Jim Dye, personal communication, November, 2001]. Thus, the size distributions used here are restricted to the Forward Scattering Spectrometer Probe (FSSP -- covering the smallest particles, from a few micrometers to about 55 µm) and the Two-Dimensional optical array Cloud probe (2D-C -- from about 55 µm to 1 mm, with estimates from reconstruction of "cropped" images to as large as 4 mm, but with relatively low sensitivity to the largest particles due to limited sample volume). An example of such a

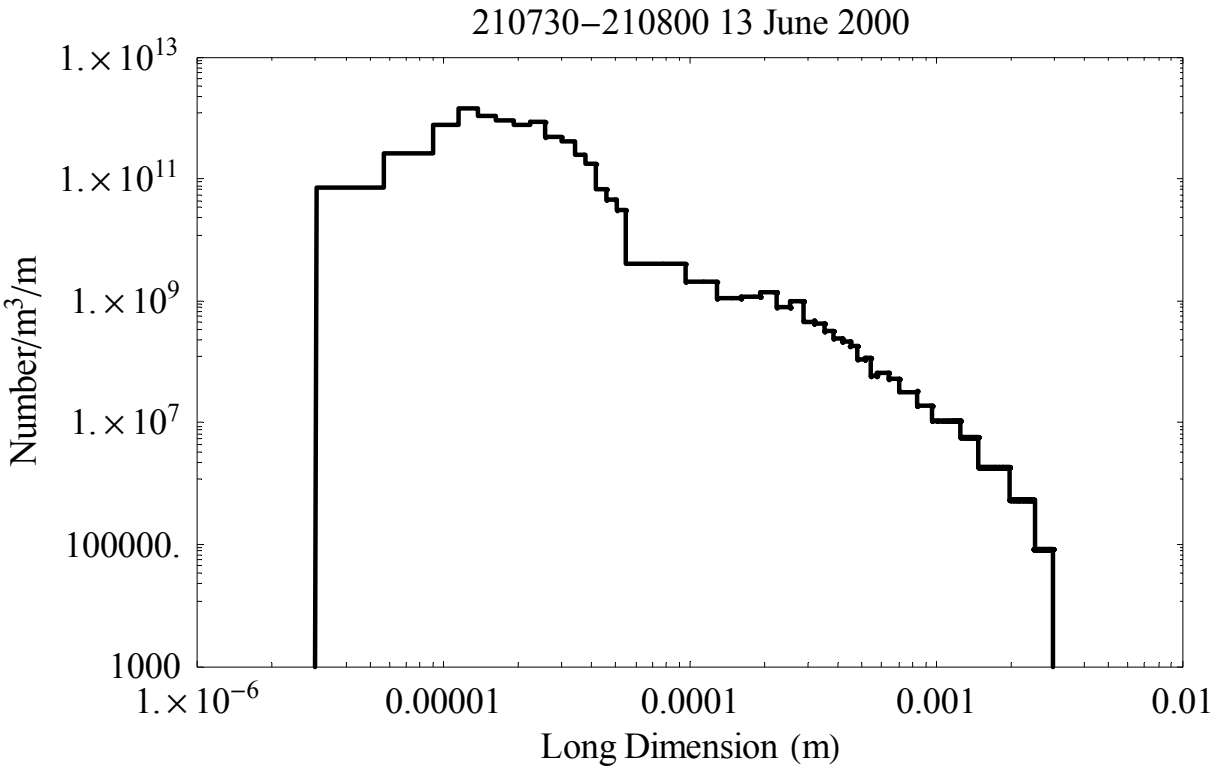

Figure 3 -- Composite Size Distribution from the FSSP and 2D-C sensors for the 30 s interval beginning at 210730 on 13 June 2000.

size distribution is given in Figure 3, which applies to a dense anvil that was penetrated at an altitude of 10.0 km, only about 25 km downwind from the core of a still-active thunderstorm.

Particles were counted in pre-defined size bins by each instrument, and this "bar-graph" representation was used explicitly in the software described herein, as reflected in Figure 3. The size spectrum has been set to zero below the smallest size bin of the FSSP and above the largest size bin with any counts from the 2D-C. This upper 2D-C cutoff varied from pass to pass, depending on the concentrations of the largest particles, since a single count corresponds to 2.3

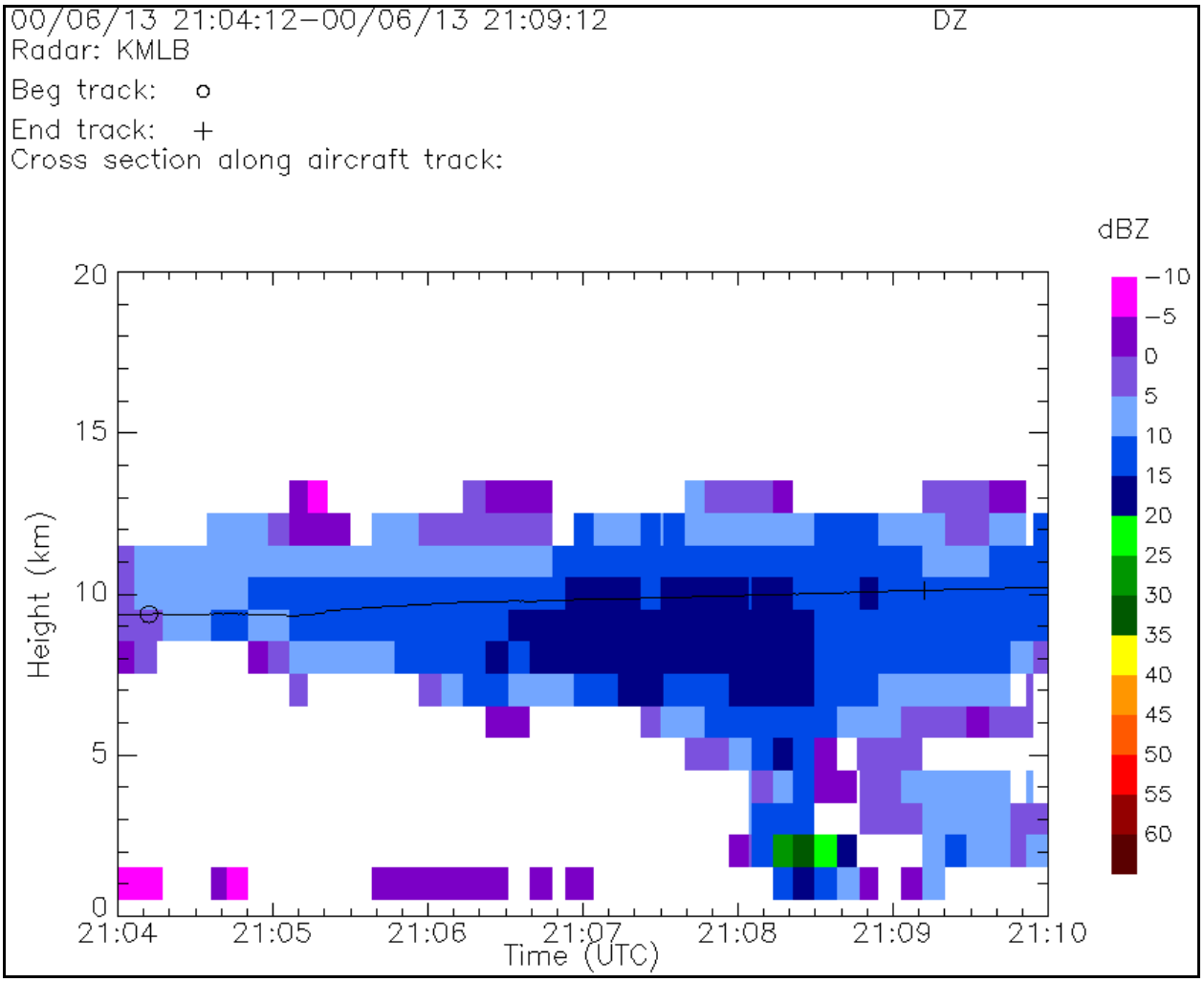

Figure 4 -- NEXRAD radar "curtain" along the flight path during the penetration containing the interval, 210730-210800, on 13 June 2000 [NCAR ABFM Web page, December, 2001]. The flight track is shown as a near-horizontal black line.

particles/m^3 in any given bin. (Based on the width of the first empty bin in Figure 3, this threshold corresponds to a spectral density of 4.5 X 10^3 particles/m^4/m centered at a size of 3.2 mm.)

The example in Figure 3 was chosen for illustration because it represents one of the highest particle concentrations and strongest radar returns encountered in the massive anvil of 13 June 2000. Thus, it probably serves as a reasonable "worst-case scenario" for the electrical decay time. Figure 4 shows the NEXRAD radar "curtain" along the flight path during this pass. At the time of the size spectrum shown in Figure 3, the aircraft was penetrating the upper part of the maximum-reflectivity region (radar echo greater than 15 dBZ) in a deep and/or precipitating cloud. The vertical electric-field intensity was approximately 30 kV/m [NCAR ABFM Web page, December, 2001]. (Note that the values of electric field quoted here and in Table 1 below are not from the final ABFM calibration matrix and should be regarded as estimates only.)

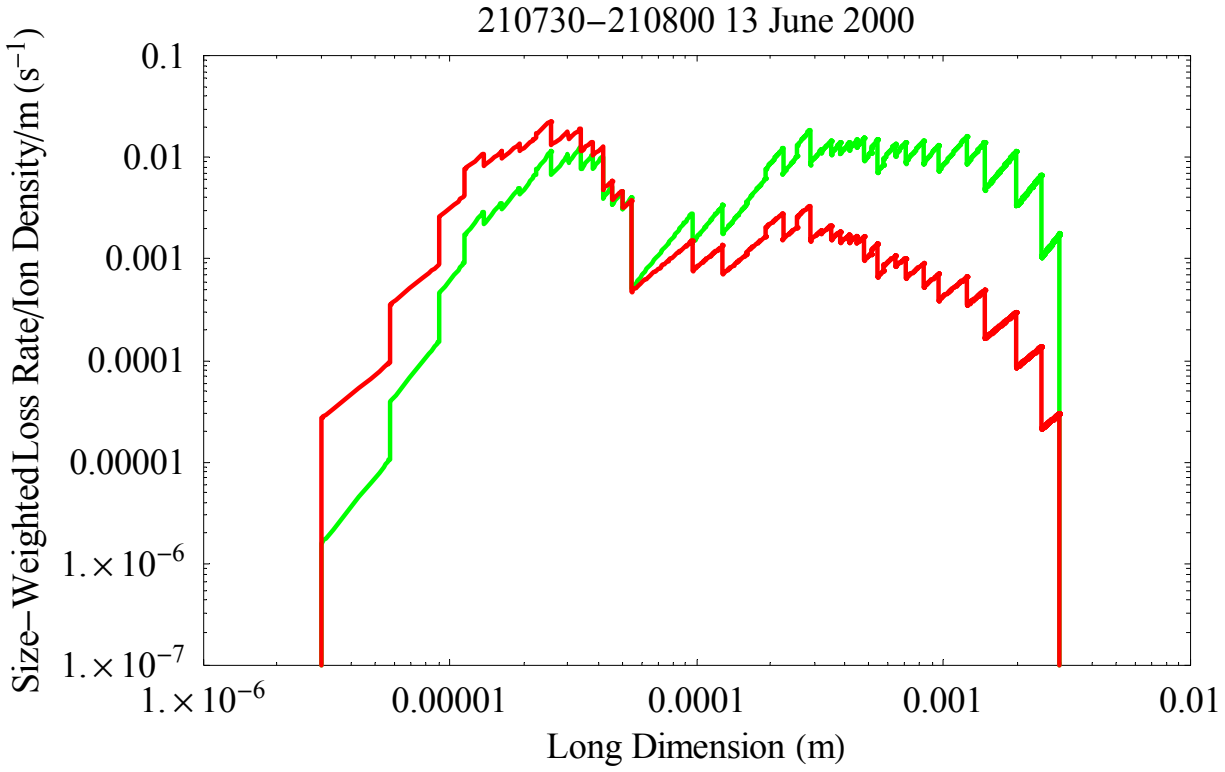

Figure 5 -- Small-ion loss rates per unit ion density and per unit particle size due to field-driven attachment in an assumed field of 1 kV/m (green) and due to diffusive attachment (red) in the interval, 210730-210800, on 13 June 2000. Note that these loss rates have been weighted by particle size to compensate for the logarithmic abscissa.

From the particle size distribution in Figure 3 it is easy to calculate size spectra of the small-ion loss rates that are modeled by the two terms on the right-hand side of Equation 2. Per unit small-ion density -- that is, with $n(t)$ cancelled out -- the field-driven-attachment rate is shown in green, and the diffusive-loss term is shown in red, in Figure 5. To compute the former, it is necessary to assume an electric-field intensity, here taken as 1 kV/m. (The only effect of changing the ambient field is to shift the green curve vertically in proportion to E.) Each of these loss terms has been multiplied by the particle long dimension, y, to compensate for the effect of the logarithmic size axis. Thus, the units of these size-weighted spectral loss rates are simply inverse seconds. This weighting is convenient because larger magnitudes on the graph make larger contributions to the total ion-loss rate (the integral over particle size).

As expected from the size dependences of A_e and C, diffusive loss dominates at small particle sizes, whereas field-driven loss dominates at large sizes. The field-dependent cross-over size can be determined from the condition, $\gamma = 1$, as discussed

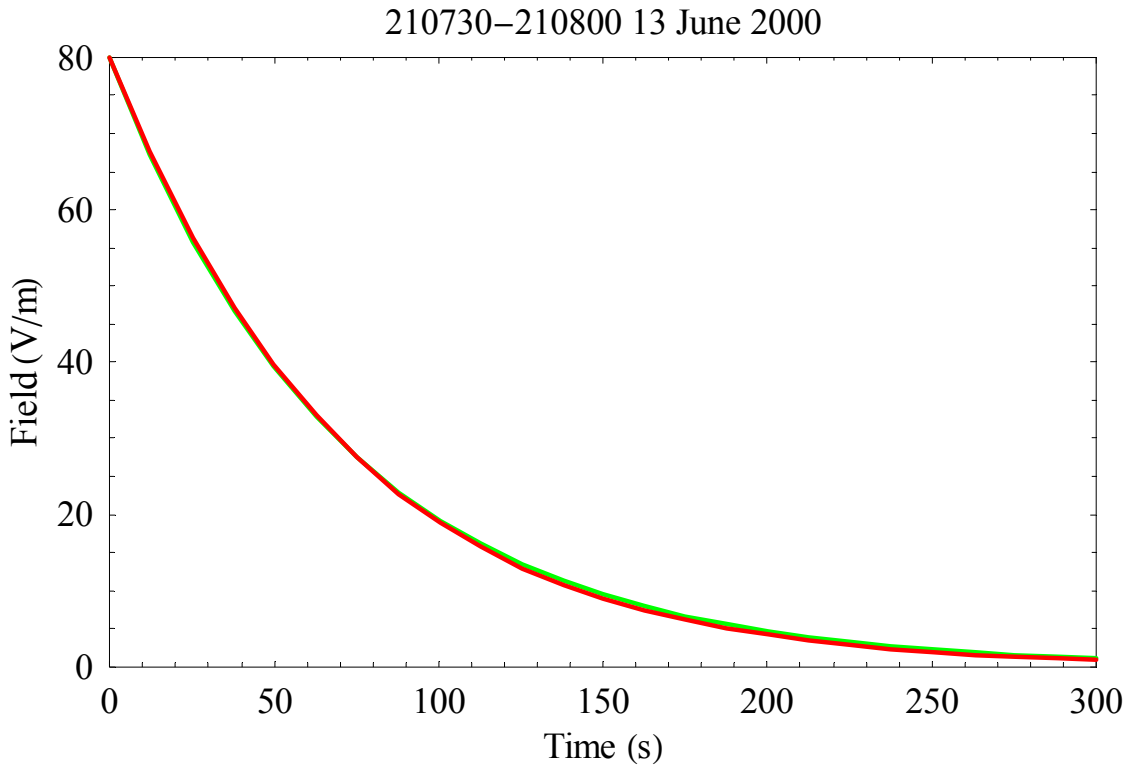

Figure 6 -- Ambient-field decay in the "low-field limit." The red curve is the model result from solution of Equation 5, using the size distribution of Figure 3. The green curve is a true exponential decay fitted to the points at E_0 and E_0/Exp(1) on the red curve.

earlier. Notice that the total diffusive loss rate (the integral of this term over size) is dominated by particles in the 10-50 μm range, as is almost always the case in this data set. (This result might change somewhat, however, when ventilation effects are included.) The total field-driven loss rate, on the other hand, is dominated by particles larger than 200 μm. Fortunately, the 2D-C data extends to large enough sizes to make it clear that this integral is bounded by a rapid decrease in concentration of particles larger than 2 mm. This may not always be the case, so HVPS data may be necessary for certain passes.

Returning to Equation 5, we can integrate the two loss terms in the denominator over particle size and then solve the non-linear, first-order, ordinary differential equation for $E(t)$, given the initial condition, E_0, at $t = 0$. Looking first at the low-field limit (E_0 = 80 V/m), where diffusive loss dominates at all significant particle sizes, we find the near-exponential decay shown by the red curve in Figure 6. The time constant of the fitted exponential, shown in green, is τ_D = 70.4 s, which is long enough compared to $\tau_e \approx 19$ s that diffusive attachment clearly dominates the neglected small-ion recombination in this case.

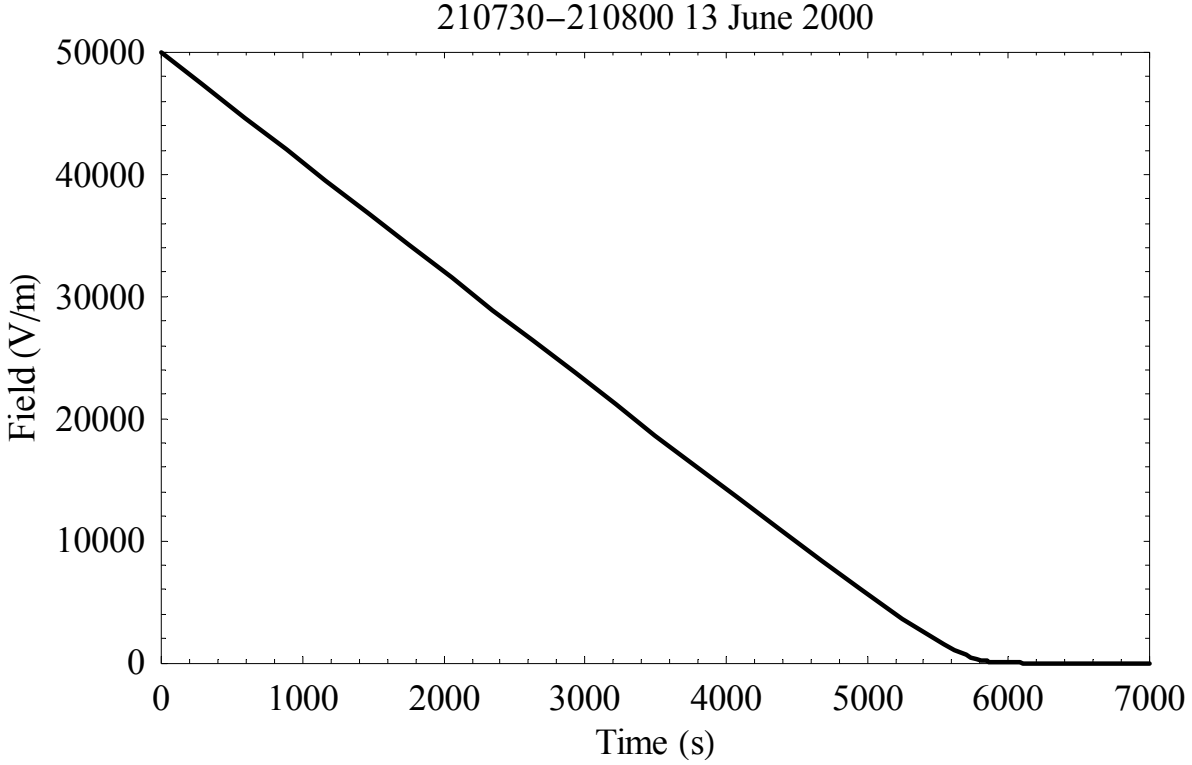

Figure 7 -- Ambient-field decay in the "high-field limit." The result from solution of Equation 5 using the size distribution of Figure 3.

The time scale indicated by Figure 6 is insignificant from the point of view of launch safety, but in the high-field limit the electrical decay is very much slower, as shown in Figure 7. Here the numerical solution to (5) has been started from an initial ambient field of E_0 = 50 kV/m at t = 0. As expected from *Krehbiel* [1967] and the discussion above, the field decreases almost linearly to relatively low values. Extrapolation of this linear decay to $E(\tau_E)$ = 0 yields a more relevant time scale, τ_E = 5569 s, which is in excess of 1-1/2 hours! This is clearly comparable to the waiting times prescribed by the current LCC, but as we shall see later, it is probably an extreme upper bound for anvil clouds far down wind from the parent storm.

A closer look at the transition between the high-field and low-field limits is provided by Figure 8, which shows a blow-up of the region of Figure 7 near $t = \tau_E$. Note that the model field decay, now shown in red, appears approximately linear down to 2 kV/m, although it deviates significantly from the linear extrapolation, shown in green, below about 10 kV/m. The model decay becomes roughly exponential below 300 V/m.

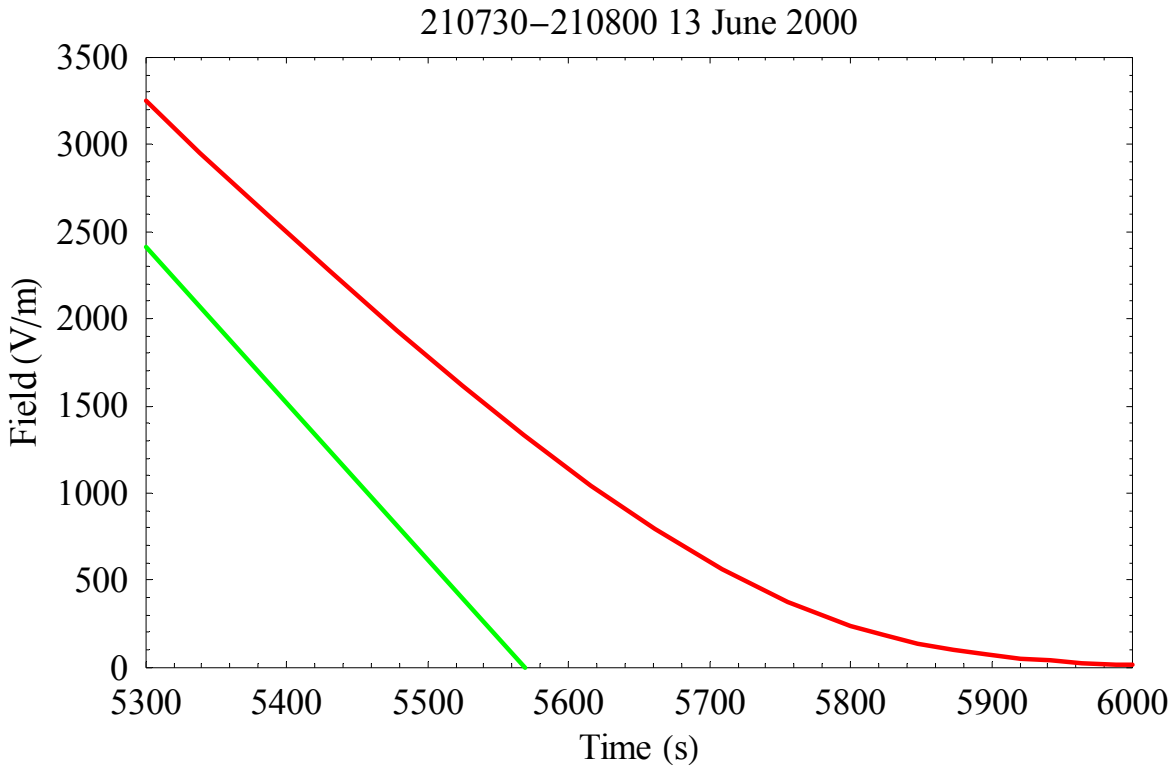

Figure 8 -- Expanded version of Figure 7 near τ_E = 5569 s. The red curve is the model result; the green curve is a true linear decay fitted to the points at E_0 and $E_0/2$ on the model decay.

Seven additional cases from 13 June 2000 have been analyzed in an effort to span the observed conditions in this anvil cloud. All eight cases are summarized in Table 1, which lists the following observations at the aircraft: estimated NEXRAD radar reflectivity and approximate vertical electric-field magnitude, from the NCAR ABFM Web page [December, 2001], and total particle concentrations (given in more conventional units in this table only) from the FSSP between 3.01 and 54.56 μm, from the 2D-C between 54.56 μm and 4 mm, and counting only those particles larger than 960 μm from the 2D-C. Also listed are the model-calculated electrical-relaxation time constant in the low-field limit, τ_D, and linear electrical-decay time scale in the high-field limit, τ_E.

Table 1 -- Summary of observations and calculations for 30 s intervals starting at the indicated times on 13 June 2000, listed in descending order of τ_E (last column). The values of electric field quoted here are not from the final ABFM calibration matrix and should be regarded as estimates only. The parentheses around most values of τ_D signify that these numbers are under-estimates because small-ion recombination losses have been neglected. The asterisk indicates that this value of τ_E is under-estimated because the 2D-C data do not extend to large enough particle sizes.

Time (HHMMSS)	NEXRAD (dBZ)	Field (kV/m)	FSSP (#/cc)	2D-C (#/l)	> 960 μm (#/l)	τ_D (s)	τ_E (s)
210730	15-20	30	23.2	497	5.67	70.4	5569
215500	15	30	25.0	449	5.86	58.7	4940
214800	15	25	7.89	205	3.43	(15.4)	2329
235200	10	few	3.05	49.4	0.956	(15.7)	1426
225100	15	50	3.74	51.1	1.26	(13.4)	1123*
232030	5-10	few	2.21	39.9	0.804	(8.15)	750
230030	0	near 0	0.643	14.2	0.334	(2.29)	240
224100	< -10	near 0	0.565	29.2	< .0023	(1.45)	91

In Table 1 it is striking that (except for the interval, 225100-225130) radar reflectivity, ambient field, nearly all the values of particle concentration in the three size ranges, and nearly all the values of τ_D decrease monotonically with decreasing τ_E. Strong correlations among the observed parameters, notably electric field vs. radar reflectivity and field vs. particle concentrations, have already been pointed out by *Dye* [2001]. In this report attention is directed instead toward the apparently strong correlations between computed τ_E and the various observations in the table. The asterisk on the value of τ_E for the deviant interval, 225100-225130, indicates that the size-weighted spectrum of small-ion loss rate due to field-driven attachment (that plotted green in Figure 5 for a different case) does not decrease toward the upper 2D-C cutoff.

Were HVPS data available in this case, τ_E would probably be found appreciably larger than indicated. An anomalously large ambient field was also observed in this case, probably related to a thick layer of unusually high reflectivity (> 25 dBZ) below the aircraft.

One other case in Table 1 deserves detailed comment. At the opposite extreme from the dense, highly-electrified anvil at 210730-210800 (see Figures 3-8) is the tenuous, un-electrified case at 224100-224130. In this interval the aircraft was penetrating an anvil over KSC, some 110 km downstream from the decaying core of the parent storm. An observer at the Range Operations Control Center characterized this cloud as "opaque" [Jim Dye, personal communication, November, 2001], although it showed no detectable radar return on the NEXRAD. The flight level of 10.6 km might have been above the densest part of this cloud, but particles were nevertheless detected in all size bins below 960 µm.

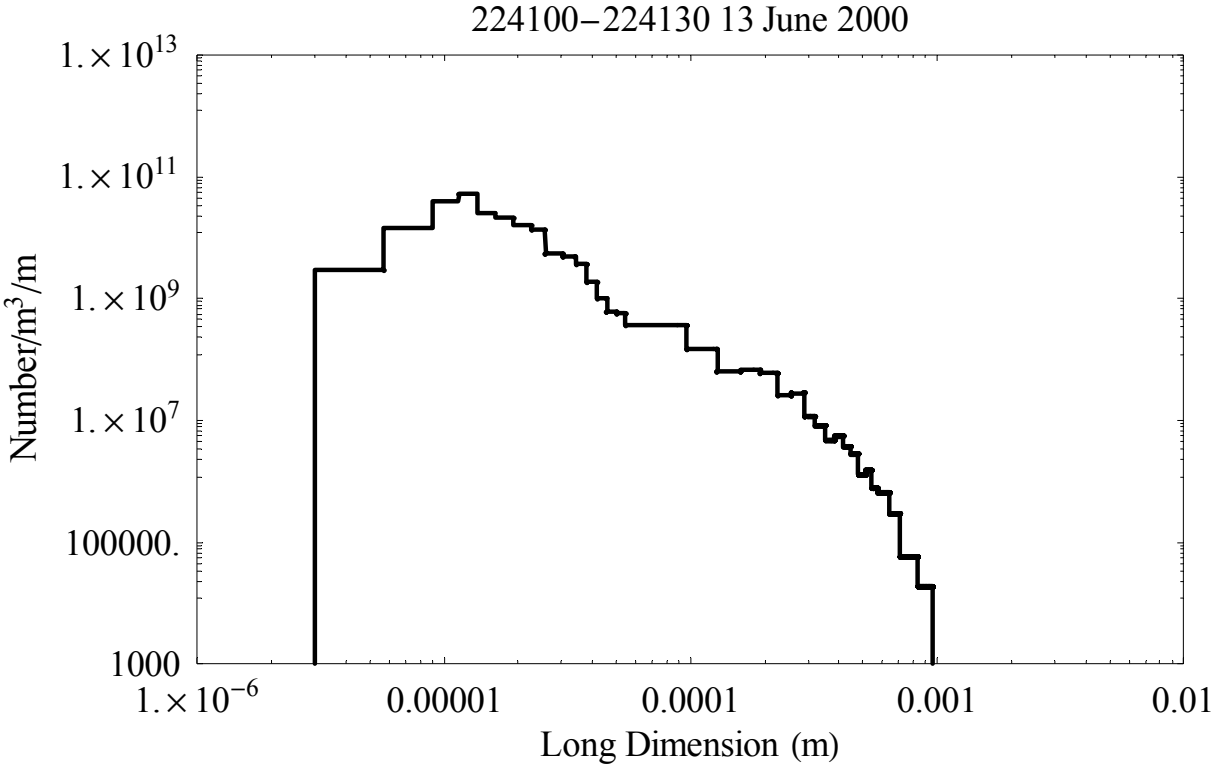

Figure 9 -- Composite Size Distribution from the FSSP and 2D-C sensors for the 30 s interval beginning at 224100 on 13 June 2000.

The size distribution at 224100-224130 is shown in Figure 9. Comparison with Figure 3 reveals a similar shape between 3.01 and about 500 µm, although the spectral densities are

between one and two orders of magnitude smaller in the present case. Above 500 µm the spectrum falls much more steeply here, however, probably because this is a substantially older cloud from which the largest particles have fallen out.

The effect of the dramatically steeper size spectrum above 500 µm in Figure 9 upon the small-ion loss rates is evident in Figure 10. Comparison with Figure 5 reveals that the field-driven-attachment loss rate effectively cuts off around 600 µm in the present case, whereas this same loss rate remains significant up to about 2.5 mm in the previous example. This difference is partially compensated by a relatively higher particle concentration in the 50 to 300 µm size range here. Nevertheless, Table 1 shows that the relative reduction between these two cases of the high-field electrical-decay time scale, τ_E, is greater than that of the low-field electrical-relaxation time, τ_D, by about 26%. Whatever the reason, the 91 s decay time modeled in this tenuous but "opaque" anvil is utterly negligible in the context of launch safety.

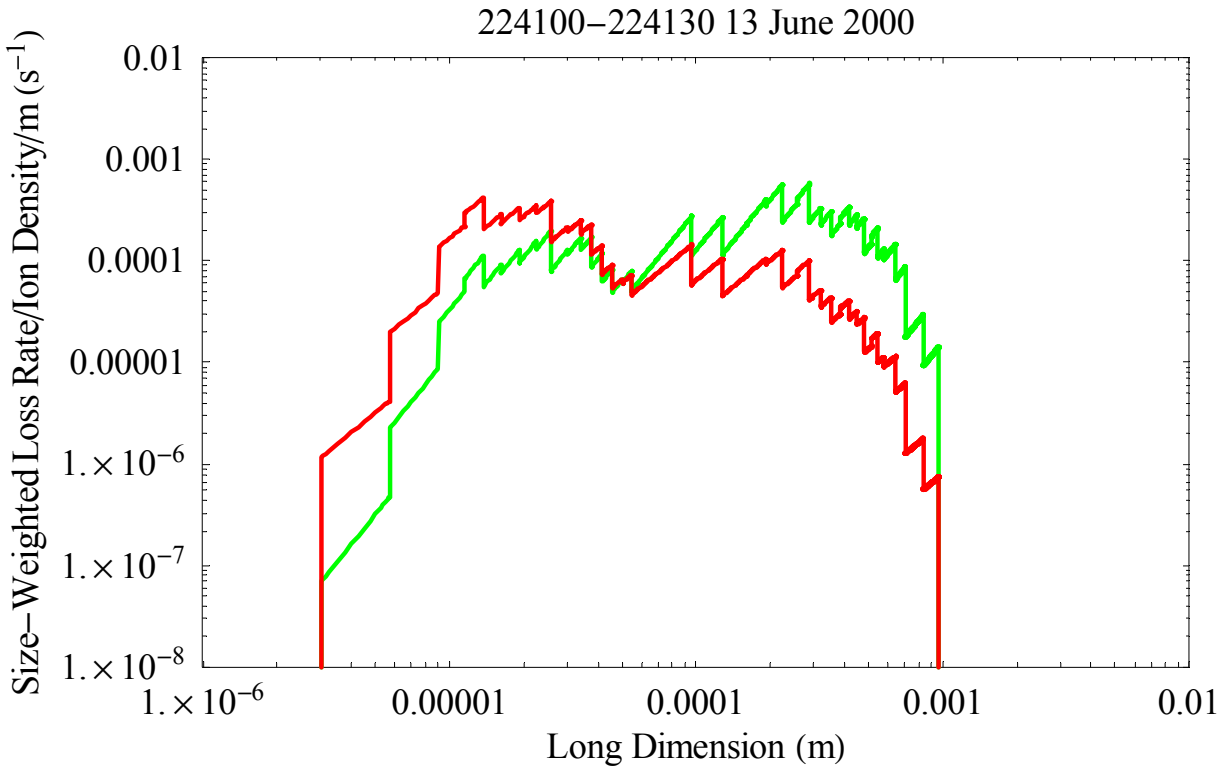

Figure 10 -- Weighted small-ion loss rates due to field-driven attachment (green) and diffusive attachment (red), as in Figure 5.

Preliminary Conclusions

Much remains to be done before final conclusions can be presented (in my second contract report). Most importantly, several cases from the 2001 campaigns that include HVPS spectra must be analyzed to make sure that the 2D-C is not missing significant numbers of large particles that could appreciably lengthen τ_E. Ventilation effects on the diffusive-loss rate must also be estimated to verify that diffusion remains negligible in the context of launch safety. Finally, with Jim Dye's help I hope to follow the decay of electric field in specific cloud parcels in an attempt to verify the model predictions against *in situ* observations.

Other important investigations that are beyond the scope of this contract include relating the measured particle-size distributions in anvil clouds (and the corresponding electrical decay rates predicted by the model) to visual observations and to radar reflectivities. Such studies are needed to establish one or more ground-based proxy measures of the electrical decay rates for use during launch operations. Initially it was expected that optical observations would be the most relevant in this regard, since the electrical decay time in the high-field limit seems closely related to the optical extinction coefficient at visible wavelengths (not measured in the ABFM campaigns) [*Krehbiel*, 1998; *Willett*, 2000]. Nevertheless, the results in Table 1 above suggest a good correlation between electrical decay time and 10 cm radar reflectivity. (Data from the 5 cm radar at Patrick AFB was not available on 13 June 2000.)

This surprising correlation, if valid, might be due to some characteristic common to all size distributions in anvil clouds. If, for example, the concentration of particles in the 200 μm to 2.5 mm size range (those apparently controlling the field-driven-attachment loss of small ions -- see Figures 5 & 10) tends to vary with the concentration of the largest particles in the cloud (those producing the radar return), then such a correlation would be expected. Further evidence that particle concentrations tend to be correlated across broad intervals of the size spectrum can be found by comparing the particle counts in the three size ranges listed in Table 1, although there are notable exceptions. This might be a productive topic for further research.

The main results of the modeling work to date are summarized in Table 1. Eight cases have been analyzed from the storm on 13 June 2000, spanning the range of radar reflectivity from greater than 15 dBZ to less than -10 dBZ. Based on these results, the following tentative conclusions are offered:

1) It is possible to explain long electrical decay times (≥ 1.5 hr.) in terms of measured particle-size spectra in especially dense anvil clouds. (This conclusion is subject to model validation against *in situ* observations of electric-field decay. A more accurate representation of the shapes of the larger particles may be necessary to accomplish this.)

2) Diffusive attachment of small ions to cloud particles is not important, as it is not capable of producing operationally significant (*i.e.*, long) electrical decay times in anvil clouds. (This conclusion is subject to assessment of the ventilation correction.)

3) Field-driven attachment can apparently produce operationally significant decay times (≥ 30 min.) only in clouds with appreciable concentrations (≥ 25/l) of particles larger than 200 μm. (This conclusion is subject to analysis of additional cases with HVPS data.)

4) The model electrical decay time appears related to the 10 cm radar reflectivity in anvil clouds, with a threshold of 10 dBZ possibly separating safe from potentially hazardous cases. (This conclusion cannot be validated in the present study, however, but requires the support of further research, as indicated above. The apparent relationship will remain essentially statistical in the absence of any accepted theoretical basis.)

Acknowledgments

I am especially grateful to Jim Dye for an introduction to the functioning (and malfunctioning) of the various microphysical instruments, for recommending both the storm and the individual cloud passes of greatest interest, for providing the size distributions used in this study, and for many constructive comments on earlier versions of the manuscript. This work would not have been possible without the dedicated field, calibration, and analytical efforts of the entire ABFM team. It was greatly facilitated by the timely presentation of ABFM results on the NCAR web site. Thanks are also due to Paul Krehbiel for pointing out the essential physics of the high-field limit and to Phil Krider for many helpful discussions and suggestions during model development. Finally, I appreciate the opportunity provided by NASA/KSC to work on this project.

List of Symbols

A_e Electrical effective area of a cloud particle
C Electrical capacitance of a cloud particle
$E(t)$ Time-dependent, vertical, electric-field intensity inside the cloud
E_0 Initial electric-field intensity
e Charge on the electron
H Vertical cloud thickness
h Screening-layer thickness
$J(t)$ Time-dependent, vertical, electric-current density inside the cloud
K Boltzmann constant
k Small-ion electrical mobility
$N(y)$ Cloud-particle volume concentration per unit size
$n(t)$ Time-dependent, small-ion volume density inside the cloud
q Small-ion volume production rate per unit volume
r Ratio of longest to shortest dimension of a cloud particle (major- to minor-axis ratio for a spheroid)
T Absolute temperature
t Time
v Horizontal cloud-advection speed
x Horizontal down-stream distance
y Longest dimension of a cloud particle (diameter for a sphere)
γ Dimensionless ratio of field-driven to diffusive ion-loss rates
ε_0 Dielectric permittivity of free space
σ_0 Initial charge horizontal-area density
τ_D Diffusion-dominated electrical-relaxation time constant in the low-field limit
τ_E Time scale for field-driven-attachment-dominated linear electrical decay in the high-field limit
τ_e Electrical-relaxation time constant in the free atmosphere
τ_i Small-ion lifetime
τ_s Screening-layer time constant

References

Brown, K.A., P.R. Krehbiel, C.B. Moore, and G.N. Sargent, Electrical screening layers around charged clouds, *J. Geophys. Res.*, *76*, 2825-2835, 1971.

Caranti, J.M., and A.J. Illingworth, Frequency dependence of the surface conductivity of ice, *J. Phys. Chem.*, *87*, 4078-4083, 1983.

Dye, J.E., Unpublished presentation at the AMFM Workshop, Cocoa Beach, FL, November 27-28, 2001.

Gaskell, W., A laboratory study of the inductive theory of thunderstorm electrification, *Quart. J. Roy. Met Soc.*, *107*, 955-966, 1981.

Griffiths, R.F., J. Latham, and V. Myers, The ionic conductivity of electrified clouds, *Q. J. Roy. Met. Soc.*, *100*, 181-190, 1974.

Gross, G.W., Role of relaxation and contact times in charge separation during collision of precipitation particles with ice targets, *J. Geophys. Res.*, *87*, 7170-7178, 1982.

Gunn, R., Diffusion charging of atmospheric droplets by ions, and the resulting combinations coefficients, *J. Atmos. Sci.*, *11*, 339-347, 1954.

Gunn, R., The hyperelectrification of raindrops by atmospheric electric fields, *J. Atmos. Sci.*, *13*, 283-288, 1956.

Hake, R.D. Jr., E.T. Pierce, and W. Viezee, Stratospheric Electricity, Final Report on SRI Project 1724, Stanford Research Institute, Menlo Park, CA, January, 1973.

Hoppel, W.A., and B.B. Phillips, The electrical shielding layer around charged clouds and its role in thunderstorm electricity, *J. Atmos. Sci.*, *28*, 1258-1271, 1971.

Klett, J.D., Ion transport to cloud droplets by diffusion and conduction, and the resulting droplet charge distribution, *J. Atmos. Sci.*, *28*, 78-85, 1971.

Klett, J.D., Charge screening layers around electrified clouds, *J. Geophys. Res.*, 77, 3187-3195, 1972.

Krehbiel, P.R., Conductivity of clouds in the presence of electric fields, unpublished manuscript, NMIMT, September 14, 1967.

Krehbiel, P.R., Unpublished discussion with the Lightning Advisory Panel, Tucson, AZ, January, 1998.

Krider, E.P., H.C. Koons, R.L. Walterscheid, W.D. Rust, and J.C. Willett, Natural and triggered lightning launch commit criteria (LCC), Rept. No. TR-99(1413)-1, The Aerospace Corporation, El Segundo, CA, 15 January 1999.

Latham, J., and B.J. Mason, Electrical charging of hail pellets in a polarizing electric field, *Proc. Roy. Soc. (London), A266*, 387-401, 1962.

Pruppacher, H.R., and J.D. Klett, *Microphysics of Clouds and Precipitation*, D. Reidel Publishing Company, Dordrecht:Holland, 1978.

Richards, W.G., A.W. Macafee, and J.V. Iribarne, Field-controlled ionic charging of ice crystals, *J. Geophys. Res., 86*, 3199-3202, 1981.

Whipple, F.J.W., and J.A. Chalmers, On Wilson's theory of the collection of charge by falling drops, *Quart. J. Roy. Met Soc., 70*, 103-119, 1944.

Willett, J.C., Electrical decay times in clouds, presented to the Lightning Advisory Panel, Kennedy Space Center, January, 2000.

Wilson, C.T.R., Some thundercloud problems, *J. Franklin Inst., 208*, 1-12, 1929.